Available online at www.sciencedirect.com
SCIENCE DIRECT®
ELSEVIER
International Journal of Solids and Structures 43 (2006) 4917–4936
INTERNATIONAL JOURNAL OF SOLIDS and STRUCTURES
www.elsevier.com/locate/ijsolstr

An elastic–plastic crack bridging model for brittle-matrix fibrous composite beams under cyclic loading

Andrea Carpinteri, Andrea Spagnoli *, Sabrina Vantadori

Department of Civil and Environmental Engineering and Architecture, University of Parma, Parco Area delle Scienze 181/A, 43100 Parma, Italy

Received 8 April 2005; received in revised form 20 June 2005
Available online 24 August 2005

Abstract

A fibrous composite beam with an edge crack is submitted to a cyclic bending moment and the crack bridging actions due to the fibers. Assuming a general elastic-linearly hardening crack bridging model for the fibers and a linear-elastic law for the matrix, the statically indeterminate bridging actions are obtained from compatibility conditions. The elastic and plastic shake-down phenomena are examined in terms of generalised cross-sectional quantities and, by employing a fatigue crack growth law, the mechanical behaviour up to failure is captured. Within the framework of the proposed fracture mechanics-based model, the cyclic crack bridging due to debonding at fiber–matrix interface of short fibers is analysed in depth. By means of some simplifying assumptions, such a phenomenon can be described by a linear isotropic tensile softening/compressive hardening law. Finally, numerical examples are presented for fibrous composite beams with randomly distributed short fibers.

Keywords: Bridged crack; Brittle-matrix fibrous composite beam; Elastic–plastic model; Fatigue crack growth; Linear hardening/softening; Cyclic loading

1. Introduction

As is well-known, by incorporating ductile fibers into the brittle matrix of a composite material, several mechanical properties can be improved (cracking resistance, ductility, impact resistance, fatigue strength). Fiber-reinforced cementitious composites are employed in an increasing amount of civil engineering structures. These materials under cyclic loading tend to develop cracks in the matrix, and such cracks are

* Corresponding author. Tel.: +39 0521 905927; fax: +39 0521 905924.
E-mail address: spagnoli@unipr.it (A. Spagnoli).

0020-7683/$ - see front matter © 2005 Elsevier Ltd. All rights reserved.
doi:10.1016/j.ijsolstr.2005.06.059

Nomenclature

a	crack depth
b	height of the beam cross-section
c_i	position of the ith reinforcement with respect to the bottom of the beam cross-section
D_f	fiber diameter
e_i	elastic part of crack opening translation at the ith reinforcement level
E	Young modulus of the matrix
E_f	Young modulus of the fibers
F_i	crack bridging force of the ith reinforcement
$F_{\mathrm{P},i}$	initial yield force of the ith reinforcement
$\overline{F}_{\mathrm{P},i}$	current yield force of the ith reinforcement
h_i	hardening modulus of the crack bridging law for the ith reinforcement
$K_{0,i}$	elastic stiffness of the crack bridging law for the ith reinforcement
$K_{t,i}$	plastic stiffness of the crack bridging law for the ith reinforcement
K_I	stress intensity factor
K_IC	critical stress intensity factor (fracture toughness)
l	embedded length of a single fiber
L_f	fiber length
M	bending moment
M_F	bending moment of either unstable fracture or crushing of the matrix
M_P	plastic bending moment
M_SD	shake-down bending moment
n	number of reinforcements intersected by the crack
N	number of loading cycles
p_i	plastic part of crack opening translation at the ith reinforcement level
P	pull-out force of a single fiber
P_P	initial yield pull-out force of a single fiber (peak load)
t	thickness of the beam cross-section
V_f	fiber volume fraction
w_i	crack opening translation at the ith reinforcement level
β	load factor
δ	pull-out translation of a single fiber
δ_P	pull-out translation of a single fiber at the initial yield pull-out force P_P
$\zeta_i = c_i/b$	relative position of the ith reinforcement with respect to the bottom of the beam cross-section
κ_i	hardening parameter of the crack bridging law for the ith reinforcement
λ_{ij}	localised compliance related to the crack opening translation at the ith reinforcement level due to a unit crack opening force $F_j = 1$ acting at ζ_j
λ_{iM}	localised compliance related to the crack opening translation at the ith reinforcement level due to a unit bending moment $M = 1$
λ_{MM}	rotational localised compliance due to a unit bending moment $M = 1$
$\xi = a/b$	relative crack depth
π_i	plastic part of crack opening translation at the ith reinforcement level, accumulated along the tensile or compressive direction
σ_P	initial yield crack bridging force per unit crack surface

τ_0	frictional bond at fiber–matrix interface
φ	rotation of the cracked beam cross-section

Subscripts

co	referring to the cut-off of crack bridging force
i	referring to the ith reinforcement intersected by the crack, with $i = 1,\ldots,n$
j	referring to the jth reinforcement intersected by the crack, with $j = 1,\ldots,n$

Superscripts

$\sim$	referring to a dimensionless (normalised) parameter
1	referring to tensile plastic deformations
2	referring to compressive plastic deformations
k	referring to the load step k

Other symbols are defined as they appear in the text.

bridged by the fibers. In order to correctly predict the fatigue life of a structural component, the effect of fiber bridging can effectively be modelled by treating the fibers as a distribution of forces acting on the crack faces. The fatigue crack growth influences the bridging actions, and causes significant changes in the mechanical properties of the above materials. Some theoretical models have been proposed to describe such phenomena and predict fatigue life (e.g. for metal–matrix composites with continuous fibers, see the models reported in Bao and McMeeking, 1995, and Begley and McMeeking, 1995; for cementitious composites with short fibers, see the recent models presented in Zhang and Stang, 1998, Zhang et al., 1999, and Matsumoto and Li, 1999).

In the present paper, a cracked portion of a straight beam subjected to an external cyclic bending moment and the crack bridging actions due to the fibers is analysed (Fig. 1). Assuming an elastic–plastic crack bridging model, characterised by a general linear hardening rule for the fibers and a linear-elastic law for the matrix, the statically indeterminate bridging actions are obtained from compatibility conditions related to the crack opening translations at the levels of the fibers. The elastic and plastic shake-down phenomena are examined in terms of applied bending moment against beam cross-section rotation, and the mechanical behaviour of the composite beam up to failure is captured by applying the well-known Paris fatigue crack growth law. Within the framework of the proposed fracture mechanics-based model, the cyclic crack bridging due to debonding at fiber–matrix interface of short fibers is analysed in depth. By means of some simplifying assumptions, such a phenomenon can be described by a linear isotropic tensile softening/compressive hardening law. Finally, numerical examples are presented for fibrous composite beams with randomly distributed short fibers.

The model here presented originates from previous formulations for monotonic loading applied to beams with either a single reinforcement (Carpinteri, 1984) or multiple reinforcements (Carpinteri and

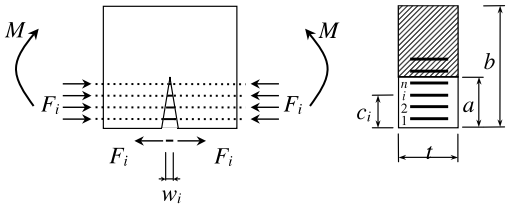

Fig. 1. Schematic of the model.

Massabò, 1996, 1997), and for cyclic loading (see Carpinteri and Carpinteri, 1984, Carpinteri, 1991, 1992, Carpinteri et al., 2005, for the case of a single reinforcement; Carpinteri and Puzzi, 2003, for the case of two reinforcements; Carpinteri et al., 2004, for the case of multiple reinforcements). The compatibility conditions considered in such papers to determine the statically indeterminate reinforcement actions are related to the rotation of the cracked beam cross-section in the case of a single reinforcement, and to crack opening translations in the case of multiple reinforcements. Further, note that the crack bridging behaviour due to the reinforcements is assumed as rigid-perfectly plastic in the above models, while it is assumed as elastic-linearly plastic in the model herein developed. This assumption allows the modelling of different types of crack bridging behaviour, like that due to short fibers (see Section 4.1) which is characterised by a softening law during tensile sliding of fibers.

2. Theoretical model

2.1. Basic framework

Consider a cracked portion of a unidirectional reinforcement composite straight beam with a rectangular cross-section under bending moment M (Fig. 1), which is cyclically varied from $M_{\min}$ to $M_{\max}$ (constant amplitude cycles). The crack presents a depth a, and is assumed to be subjected to Mode I loading (i.e. the crack is normal to the longitudinal axis of the beam). Reinforcements are discretely distributed across the crack and oriented along the longitudinal axis of the beam. The position of the ith reinforcement ($i = 1,\ldots,n$, where n is the number of reinforcement intersected by the crack) is described by the distance c_i with respect to the bottom of the beam cross-section. Note that the reinforcement numbers are sorted according to the reinforcement positions along the beam height b, by assuming that reinforcement no. 1 is the nearest to the bottom of the beam cross-section. Further, the relative crack depth $\xi = a/b$ and the normalised coordinate $\zeta_i = c_i/b$ are defined. As is shown in Section 4.3, reinforcements can be considered as idealised bridging elements (oriented along the longitudinal axis of the beam), which simulate the equivalent bridging action of randomly distributed short fibers.

The mechanical behaviour of the composite beam is as follows. The matrix (treated as a homogeneous and isotropic material) is assumed to present a linear elastic constitutive law, whereas the reinforcements are assumed to behave as elastic–plastic bridging elements which connect together the two crack faces.

2.2. Crack bridging law

A uniaxial elastic–plastic model with linear hardening for crack bridging due to reinforcements is adopted. For the ith reinforcement, with $i = 1,\ldots,n$, the relationship between the bridging force F_i and the crack opening translation w_i at the reinforcement level is schematically described in Fig. 2. In particular, the elastic domain is described by a linear relationship with a stiffness $K_{0,i}$, whereas the stiffness in the plastic domain is equal to $K_{t,i}^{(1)}$ and $K_{t,i}^{(2)}$ in tension and compression, respectively.

A decomposition can be applied to the total crack opening translation w_i so that $w_i = e_i + p_i$, where e_i is the elastic translation and p_i is the plastic translation. Further, the translation p_i is equal to $\pi_i^{(1)} - \pi_i^{(2)}$, where $\pi_i^{(1)}$ and $\pi_i^{(2)}$ are non-negative quantities corresponding to the plastic crack opening translations independently accumulated along the tensile and compressive direction, respectively. The bound of the elastic domain is described by the following relationship:

$$\begin{Bmatrix} \overline{F}_{\mathrm{P},i}^{(1)} \\ -\overline{F}_{\mathrm{P},i}^{(2)} \end{Bmatrix} = \begin{Bmatrix} F_{\mathrm{P},i}^{(1)} \\ F_{\mathrm{P},i}^{(2)} \end{Bmatrix} + \begin{bmatrix} h_i^{(1)} & \kappa_i h_i^{(2)} \\ \kappa_i h_i^{(1)} & h_i^{(2)} \end{bmatrix} \begin{Bmatrix} \pi_i^{(1)} \\ \pi_i^{(2)} \end{Bmatrix} \tag{1}$$

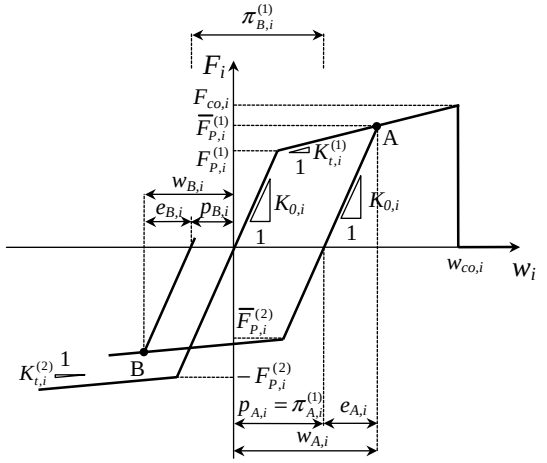

Fig. 2. Elastic–plastic model with a general linear hardening rule describing the relationship between the reinforcement bridging force F_i and the crack opening translation w_i at the reinforcement level for the generic ith reinforcement.

where $F^{(l)}_{\mathrm{P},i}$ and $\overline{F}^{(l)}_{\mathrm{P},i}$ (with $l=1$ and $l=2$ for tension and compression, respectively) are the initial and current yield forces for the ith reinforcement ($F^{(l)}_{\mathrm{P},i}$ is a non-negative quantity), κ_i is a parameter characterising the hardening law, and $h^{(1)}_i$ and $h^{(2)}_i$ are the hardening moduli given by:

$$h^{(l)}_i = K^{(l)}_{t,i}\frac{K_{0,i}}{K_{0,i}-K^{(l)}_{t,i}} \quad (l=1,2) \tag{2}$$

where $h^{(l)}_i > 0$ corresponds to (positive) hardening, and $h^{(l)}_i < 0$ corresponds to softening (negative hardening).

Depending on the values of the parameters in Eq. (1), different types of plastic behaviour can be considered. As far as $h^{(1)}_i$ and $h^{(2)}_i$ are concerned, we may have:

(i) $h^{(1)}_i > 0, h^{(2)}_i > 0$ tensile/compressive hardening,
(ii) $h^{(1)}_i < 0, h^{(2)}_i < 0$ tensile/compressive softening,
(iii) $h^{(1)}_i > 0, h^{(2)}_i < 0$ tensile hardening/compressive softening,
(iv) $h^{(1)}_i < 0, h^{(2)}_i > 0$ tensile softening/compressive hardening.

Note that, for negative values of $h^{(1)}_i$ and/or $h^{(2)}_i$, the Drucker's stability postulate is not fulfilled (e.g. see Jirasek and Bazant, 2002). On the other hand, for $|h^{(1)}_i| + |h^{(2)}_i| > 0$ the following hardening rules may be considered by varying the hardening parameter:

(i) $\kappa_i = 1$ isotropic hardening,
(ii) $\kappa_i = -1$ kinematic hardening,
(iii) $-1 < \kappa_i < +1$ cyclic hardening,
(iv) $\kappa_i = 0$ Koiter hardening.

In the proposed elastic–plastic crack bridging model, a cut-off crack opening translation $w_{\mathrm{co},i}$ can be accommodated for positive values of w_i (Fig. 2) so that, if $w_i > w_{\mathrm{co},i}$, the bridging action of the ith reinforcement becomes identically null. Note that the model is physically meaningful for non-negative values of w_i,

i.e. when material overlapping along the crack faces does not occur (see Section 2.5 for some details on this aspect). Further, note that the rigid-perfectly plastic crack bridging model (symmetric in tension and compression), reported in Carpinteri et al., 2004, becomes a special case of the present model by posing: $h_i^{(1)} = h_i^{(2)} = 0, F_{\mathrm{P},i}^{(1)} = F_{\mathrm{P},i}^{(2)}, K_{0,i} \to \infty$ and $w_{\mathrm{co},i} \to \infty$.

2.3. Compatibility conditions

Since the problem being examined is statically indeterminate, the unknown bridging actions F_i (with $i = 1, \ldots, n$) on the matrix can be deduced from n kinematic conditions related to the crack opening translations (w_i, with $i = 1, \ldots, n$) at the different reinforcement levels. In particular, since the matrix is assumed to behave in a linear elastic manner, linear elastic fracture mechanics can be applied, and the crack opening translation w_i at the ith reinforcement level is computed through the superposition principle (Carpinteri et al., 2004):

$$w_i = w_{iM} + \sum_{j=1}^{n} w_{ij} = \lambda_{iM} M - \sum_{j=1}^{n} \lambda_{ij} F_j \tag{3}$$

where w_{iM} and w_{ij} are the crack opening translations produced by the bending moment M and by the generic force F_j (assumed to be positive when the jth reinforcement is under tension), respectively; the localised compliances, λ_{iM} and λ_{ij}, due to the crack, represent the ith crack opening translation for $M = 1$ and that for a unit crack opening force, $F_j = 1$, acting at ζ_j, respectively. Using the matrix formulation, the crack opening translations are given by:

$$\{w\} = \{\lambda_M\} M - [\lambda]\{F\} \tag{4}$$

where $\{w\} = \{w_1, \ldots, w_n\}^{\mathrm{T}}$ is the vector of the crack opening translations at the different reinforcement levels, and $\{F\} = \{F_1, \ldots, F_n\}^{\mathrm{T}}$ is the vector of the unknown crack bridging forces. Further, $\{\lambda_M\}$ is the vector of the localised compliances related to the bending moment M, whereas $[\lambda]$ is a symmetric square matrix of order n, whose generic element (ij) represents the localised compliance λ_j.

The unknown reinforcement actions $\{F\}$ can be determined from congruence conditions. In other words, because of the elastic–plastic crack bridging law for the reinforcements, compatibility requires that

$$\{w\} = [A]\{F\} + \{B\} \tag{5}$$

where the matrix $[A]$ is diagonal and contains the following elements: $a_{ii} = (K_{0,i})^{-1}$ in the elastic domain; $a_{ii} = (K_{l,i}^{(l)})^{-1}$ in the plastic domain ($l = 1, 2$). The vector $\{B\}$ contains the plastic part of the crack opening translations (e.g. for the generic ith reinforcement and the unloading elastic segment reported in Fig. 2: $b_i = p_{A,i}$).

By equating Eqs. (4) and (5), we have:

$$\{\lambda_M\} M - [\lambda]\{F\} = [A]\{F\} + \{B\} \tag{6}$$

and the unknown vector $\{F\}$ can be obtained from Eq. (6):

$$\{F\} = ([\lambda] + [A])^{-1}(\{\lambda_M\} M - \{B\}) \tag{7}$$

Since the matrix $[A]$ and the vector $\{B\}$ are functions of the solution vector $\{F\}$, Eq. (6) must be solved according to an incremental procedure (see Section 2.5) which accounts for the loading–unloading alternative corresponding to elastic-to-plastic transitions when $w_i \mathrm{d}w_i > 0$ ($\mathrm{d}w_i =$ increment of the total crack opening translation at the ith reinforcement level) and to plastic-to-elastic returns when $w_i \mathrm{d}w_i < 0$.

2.4. Fatigue crack growth and failure

The crack is herein assumed to propagate under cyclic loading according to the Paris law $\mathrm{d}a/\mathrm{d}N = C(\Delta K_\mathrm{I})^m$ (Paris and Erdogan, 1963). The stress intensity factor (SIF) range ΔK_I is taken as equal to $(\langle K_{\mathrm{I,max}}\rangle - \langle K_{\mathrm{I,min}}\rangle)$, where $K_{\mathrm{I,max}}$ and $K_{\mathrm{I,min}}$ are the maximum and minimum SIF value within a load cycle, and $\langle\ \rangle$ are the MacCauley brackets ($\langle x\rangle = (x + |x|)/2$). The stress intensity factor K_I is computed through the superposition principle: $K_\mathrm{I} = K_{\mathrm{I}M} - \sum_{i=1}^{n} K_{\mathrm{I}i}$, where $K_{\mathrm{I}M}$ and $K_{\mathrm{I}i}$ are due to the bending moment M and the reinforcement action F_i respectively (see Appendix A in Carpinteri et al., 2004). Note that the crack length increments due to fatigue loading imply a variation of the localised compliances.

The collapse of the beam under the applied bending moment might occur for two possible reasons: (1) unstable fracture of the matrix (when the toughness K_IC of the material is attained, that is, $K_\mathrm{I} = K_\mathrm{IC}$), or (2) crushing of the matrix (when the normal compressive stress σ_c, computed through the classical bending theory applied to the ligament, attains the material strength f_c).

2.5. Numerical procedure

The theoretical model presented above is implemented in a numerical step-by-step procedure. Accordingly, the cyclic loading history of the external bending moment is applied through finite holonomic steps, and plastic-to-elastic returns corresponding to $w_i \Delta w_i < 0$ (Δw_i = finite increment of the total crack opening translation at the ith reinforcement level) might occur at bending moment reversals. The flow-chart of the procedure is as follows:

1. Compute the localised compliances (see Eqs (A.11)–(A.13) in Carpinteri et al., 2004; Appendix A) for the beam being considered, with a given value ξ of the initial crack depth.
2. For the virgin elastic domain, initialise the matrix $[A]$ $({}^0a_{ii} = (K_{0,i})^{-1}; i = 1,\ldots,n)$, the vector $\{B\}$ $({}^0b_i = 0; i = 1,\ldots,n)$, the plastic crack opening translations $({}^0\pi_i^{(l)} = 0; i = 1,\ldots,n;\ l = 1,2)$ and the bounds of the elastic domain $({}^0\overline{F}_{\mathrm{P},i}^{(l)} = F_{\mathrm{P},i}^{(l)}$ from Eq. (1); $i = 1,\ldots,n;\ l = 1, 2)$.
3. At the generic load step k, determine the solution vector $\{{}^kF\}$ from Eq. (7), by posing either $M = M_{\max}$ (during loading) or $M = M_{\min}$ (during unloading). If at least one of the crack opening translations at the reinforcement levels (obtained from Eq. (5)) attains a negative value, the solution vector $\{{}^kF\}$ results to be physically meaningless (because of material overlapping along the crack surfaces), and the numerical procedure stops.
4. Calculate the load factor ${}^k\beta$ for which the most highly stressed *elastic* reinforcement is on the verge of its elastic domain:

$$ {}^k\beta = \max_{1\leqslant i\leqslant n}\left\{\frac{{}^kF_i - {}^{k-1}F_i}{{}^{k-1}\overline{F}_{\mathrm{P},i}^{(l)} - {}^{k-1}F_i}\right\} \quad \text{if } {}^{k-1}\overline{F}_{\mathrm{P},i}^{(l)} - {}^{k-1}F_i \neq 0 \tag{8}$$

   where $l = 1$ during loading, and $l = 2$ during unloading. Note that, when the ${}^k\beta$ value computed from Eq. (8) results to be lower than 1 (that occurs when there is no new reinforcement yielding during the load step k), the load factor is posed as equal to the unity (see Eqs. (9) and (10) below, to better understand such a position). In the case that cut-off values of the bridging actions are considered, the maximisation of Eq. (8) should be made also for the ratio $({}^kF_i - {}^{k-1}F_i)/(F_{\mathrm{co},i} - {}^{k-1}F_i)$ during a loading step if ${}^{k-1}\overline{F}_{\mathrm{P},i}^{(1)} - {}^{k-1}F_i = 0$.
5. From the load factor ${}^k\beta$, calculate the bending moment ${}^kM$ for which the most highly stressed *elastic* reinforcement is on the verge of its elastic domain, namely:

$$ {}^kM = \frac{M - {}^{k-1}M}{{}^k\beta} + {}^{k-1}M \tag{9}$$

where $M = M_{\max}$ during loading and $M = M_{\min}$ during unloading. Note that, at a load step k corresponding to either a loading–unloading reversal or an unloading–reloading reversal, ${}^{k}\beta$ is equal to 1 and, according to Eq. (9), ${}^{k}M$ results to be equal to either $M_{\max}$ or $M_{\min}$, respectively. Further, at the first load step k after a loading–unloading reversal, ${}^{k-1}M$ is equal to $M_{\max}$ whereas, at the first load step k after an unloading–reloading reversal, ${}^{k-1}M$ is equal to $M_{\min}$. Then, it can be remarked that, at the very first load step (i.e. $k = 1$), ${}^{k-1}M = {}^{0}M$ is equal to 0.

6. Update the reinforcement actions:

$$\{{}^{k}F\} = \frac{\{{}^{k}F\} - \{{}^{k-1}F\}}{{}^{k}\beta} + \{{}^{k-1}F\} \tag{10}$$

7. Calculate the plastic crack opening translations ${}^{k}\pi_i^{(l)}$ $(i = 1, \ldots, n;\ l = 1, 2)$. For each reinforcement having ${}^{k}\pi_i^{(1)} > 0$ during a loading step or ${}^{k}\pi_i^{(2)} > 0$ during an unloading step, calculate its current elastic domain $({}^{k}\overline{F}_{\mathrm{P},i}^{(l)}; i = 1, \ldots, n;\ l = 1, 2$; see Eq. (1)).
8. If the *load step k does not terminate at a reversal*, update the elements ${}^{k}a_{ii}({}^{k+1}a_{ii} = (K_{t,i}^{(l)})^{-1}$ with $l = 1$ during a loading step and $l = 2$ during an unloading step) and ${}^{k}b_i$ for the ith reinforcement which is placed on the verge of its elastic domain during the load step k (elastic-to-plastic transition). If the *load step k terminates at a reversal*, update the elements ${}^{k}a_{ii}({}^{k+1}a_{ii} = (K_0)^{-1})$ and ${}^{k}b_i$ for each reinforcement having ${}^{k}\overline{F}_{P,i}^{(1)} - {}^{k}\overline{F}_i = 0$ during a loading step or ${}^{k}\overline{F}_{P,i}^{(2)} - {}^{k}\overline{F}_i = 0$ during an unloading step (plastic-to-elastic returns). If the ith reinforcement has reached the cut-off limit $({}^{k}F_i = F_{\mathrm{co},i})$, cancel out the corresponding row in the matrices and vectors of Eqs. (4)–(7).
9. Stop if $K_{\mathrm{I}} = K_{\mathrm{IC}}$ or if the compressive strength f_{c} is attained in the matrix.
10. Increase the crack length according to the Paris law and update the localised compliances. The Paris law is applied after every block of cycles. The number of cycles in each block is calculated in order to produce an increment of the crack length $\Delta\xi$ greater than a given fraction of the beam height.
11. Return to step no. 3 of the present procedure.

3. Cyclic flexural behaviour

The relative rotation φ, due to the crack only (i.e. excluding the elastic deformation of the matrix), of the two extreme cross-sections of the beam portion in Fig. 1 can be obtained as follows:

$$\varphi = \lambda_{MM} M - \{\lambda_M\}^{\mathrm{T}}\{F\} \tag{11}$$

where λ_{MM} is the rotational localised compliance due to a unit bending moment $M = 1$ (see Eq. (A.13) in Carpinteri et al., 2004; Appendix A). According to the numerical procedure outlined above, the rotation ${}^{k}\varphi$ is calculated through Eq. (11), by substituting M with ${}^{k}M$ (see Eq. (9)) and $\{F\}$ with $\{{}^{k}F\}$ (see Eq. (10)).

The overall response of the cracked beam cross-section under cyclic bending can be analysed in terms of applied bending moment M vs cross-section rotation φ curves. For a given crack depth, the most significant values of the bending moment are: the plastic bending moment M_{P} which produces the first tensile yielding in the most highly stressed reinforcement during loading; the shake-down bending moment M_{SD} above which the first compressive yielding in the most highly stressed reinforcement occurs during unloading; further, M_{F} is the bending moment of matrix unstable fracture when K_{I} attains K_{IC}, or the bending moment of matrix crushing when the compressive strength f_{c} is attained. The following regions of behaviour can be identified (Fig. 3):

(i) elastic behaviour for $0 \leqslant M_{\max} \leqslant M_{\mathrm{P}}$ (see the case related to $M'_{\max}$),
(ii) elastic shake-down for $M_{\mathrm{P}} \leqslant M_{\max} \leqslant M_{\mathrm{SD}}$ (see the case related to $M''_{\max}$),
(iii) plastic shake-down for $M_{\mathrm{SD}} \leqslant M_{\max} \leqslant M_{\mathrm{F}}$ (see the case related to $M'''_{\max}$).

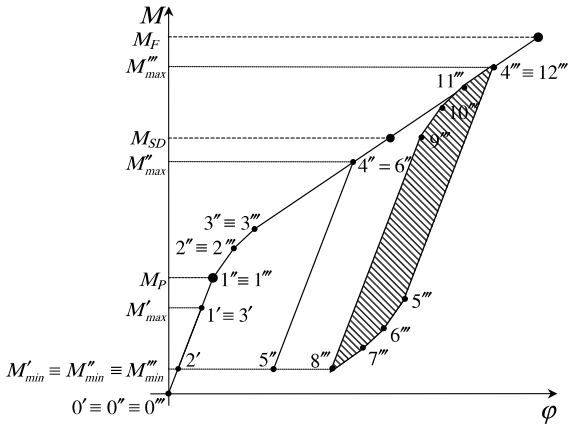

Fig. 3. Schematic of bending moment M against rotation φ cyclic curves identifying the following regions of behaviour: elastic behaviour for M ranging from $M'_{\min}$ to $M'_{\max}$ (load steps $0'$, $1'$, $2'$, $3'$); elastic shake-down for M ranging from $M''_{\min}$ to $M''_{\max}$ (load steps $0''$, $1''$, $2''$, $3''$, $4''$, $5''$, $6''$); plastic shake-down for M ranging from $M'''_{\min}$ to $M'''_{\max}$ (load steps $0'''$, $1'''$, $2'''$, $3'''$, $4'''$, $5'''$, $6'''$, $7'''$, $8'''$, $9'''$, $10'''$, $11'''$, $12'''$; the dashed area $4'''$, $5'''$, $6'''$, $7'''$, $8'''$, $9'''$, $10'''$, $11'''$, $12'''$ corresponds to the energy dissipated per cycle).

In the case of plastic shake-down, the bending moment vs rotation curve describes a hysteretic loop, and the energy dissipated per cycle is equal to the area of this loop (e.g. see the dashed area $4'''$, $5'''$, $6'''$, $7'''$, $8'''$, $9'''$, $10'''$, $11'''$, $12'''$ in Fig. 3):

$$\frac{\text{work}}{\text{cycle}} = \sum_{k=s_b}^{s_e} \frac{1}{2}({}^{k+1}M + {}^{k}M)({}^{k+1}\varphi - {}^{k}\varphi) \tag{12}$$

where s_b = load step at the beginning of the cycle, and s_e = load step at the end of the cycle (e.g. $s_b = 4'''$ and $s_e = 11'''$ in Fig. 3).

Provided that the crack depth does not change (non-propagating crack), the constant amplitude cyclic flexural behaviour discussed above in terms of bending moment M against beam cross-section rotation φ is reminiscent of that described through a classical constitutive theory for cyclic plasticity with a linear-piecewise kinematic hardening law (e.g. see Chaboche, 1986, for a review, and Masing, 1926, for his early parallel sub-element model). Therefore, no ratchetting effect (accumulated plastic deformations) is accounted for by the proposed model. This behaviour can also be demonstrated by the fact that, according to the present model, the M–φ relationship (11) depends only on the current values of the variables $[A]$ and $\{B\}$ (see Eq. (7)) and of the internal-state variables $\pi_i^{(1)}$ and $\pi_i^{(2)}$ $(i = 1, \ldots, n)$, so as to exclude any hereditary condition in the model (e.g. see Chaboche, 1986).

4. The case of short-fiber composites

Let us consider a fibrous composite material characterised by straight fibers of length L_f and diameter D_f (Fig. 4), whereas V_f is the fiber volume fraction.

4.1. Pull-out analysis of a single fiber

Consider first an isolated fiber loaded at its end with a pull-out force P acting along the fiber axis (e.g. see Marshall et al., 1985; McCartney, 1987; Li, 1992). The fiber is embedded in a matrix cylinder of diameter

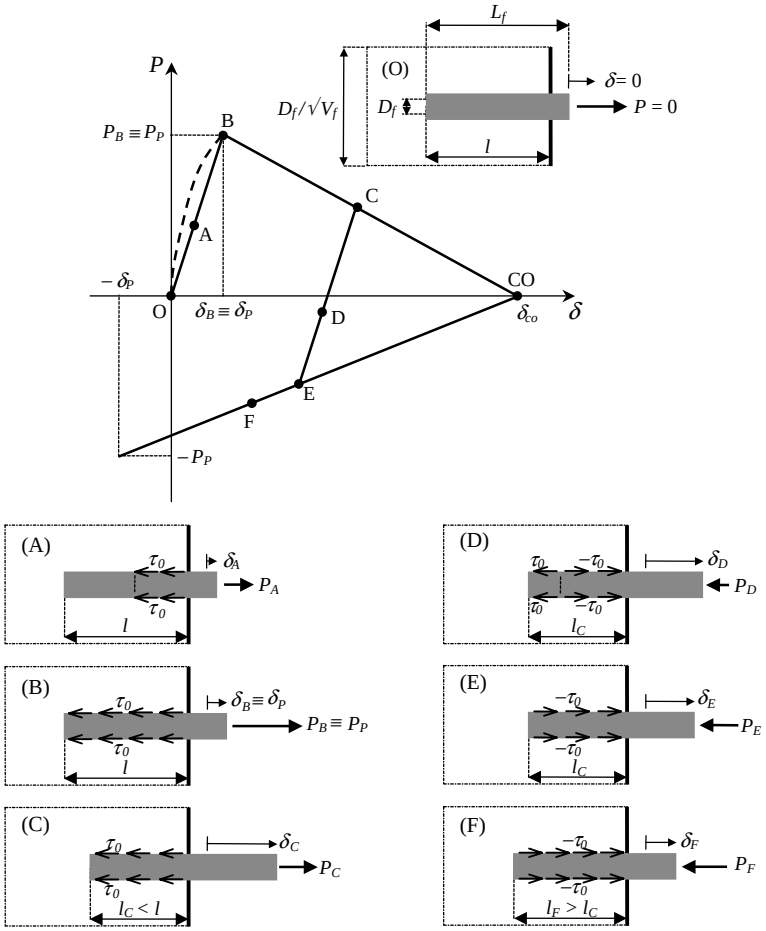

Fig. 4. Cyclic pull-out behaviour of a single aligned fiber.

$D_f/\sqrt{V_f}$ (corresponding to the fiber–matrix unit cell) (Fig. 4). Both the fiber and the matrix are taken as elastic (E and E_f are the Young modulus of the matrix and the fiber, respectively). Further, two zones are assumed along the embedded length l of the fiber: a sliding zone (understood as the activation zone of frictional sliding between fiber and matrix) characterised by a constant frictional bond stress τ_0; a non-sliding zone characterised by equal strains in both the matrix and the fiber (i.e. the effect of shear stress is neglected).

Under such hypotheses, as the force P increases, extension of the sliding zone from the free surface of the matrix cylinder occurs, and the translation δ of the loaded end of the fiber increases as a result of both the stretching of the fiber segment (along the length of the sliding zone) and the deformation of the fiber–matrix unit cell (along the length of the non-sliding zone). The P–δ relationship is as follows (Marshall et al., 1985; dashed line in Fig. 4):

$$P(\delta) = \frac{\pi}{\sqrt{2}}\sqrt{(1+\eta)E_f D_f^3 \tau_0 \delta} \tag{13}$$

where

$$\eta = (E_f V_f)/[E(1-V_f)] \tag{14}$$

Eq. (13) is valid until the sliding zone reaches the embedded end of the fiber (full debonding of the fiber), which corresponds to a pull-out translation δ_P and a force P_P given by:

$$P_P = \pi D_f l \tau_0 \tag{15}$$

The peak load P_P corresponds to the initial yield force according to the elastic–plastic crack bridging model presented above (see Section 4.3). By replacing $P(\delta)$ with P_P and δ with δ_P in Eq. (13), we obtain:

$$\delta_P = (2l^2\tau_0)/[(1+\eta)E_f D_f] \tag{16}$$

After full debonding, fiber pull-out continues, and the pull-out force decreases as a result of the decreasing embedded length of the fiber. Assuming a constant frictional bond and ignoring the elastic stretching of the fiber and the fiber–matrix unit cell at this stage, the following relationship holds (Li, 1992; solid line passing through points B and CO in Fig. 4):

$$P(\delta) = \pi D_f l \tau_0 \left(1 - \frac{\delta - \delta_P}{\delta_{co} - \delta_P}\right) \tag{17}$$

where δ_{co} is the cut-off translation (of the loaded end of the fiber) corresponding to a complete pull-out of the fiber of initial embedded length l, that is:

$$\delta_{co} = l \tag{18}$$

Eqs. (13)–(18) describe the pull-out behaviour of a single fiber under monotonic loading in its pre- and post-peak stages. The peak load P_P (Eq. (15)) can be reached without rupture of the fiber only if it is lower than $\sigma_f(\pi D_f^2/4)$, where σ_f is the fiber tensile strength. From such a condition, we obtain:

$$l \leqslant (\sigma_f D_f)/(4\tau_0) \tag{19}$$

This relationship is commonly used (posing $l = L_f$) to define the so-called short-fiber range characterised by a shear failure of the interface rather than a tensile failure of the fiber.

Within the framework of the proposed model, the non-linear expression (13) is approximated by the secant passing through point B of coordinates (δ_P, P_P) and point O (see solid line in Fig. 4 for the pre-peak stage).

Now the monotonic pull-out behaviour described above is extended to cyclic loading. To summarise, in the initial pre-peak stage (see the generic point A in Fig. 4) the load P linearly increases with increasing δ up to full debonding (point B). Afterwards, the pull-out force decreases and, at a generic load reversal (point C), the sliding direction and the frictional bond stress τ_0 start to reverse (e.g. see McMeeking and Evans, 1990). During unloading, a linear P–δ relationship is assumed to hold (see the generic point D) until the reversed sliding zone reaches the embedded end of the fiber (full reversed debonding of the fiber of embedded length l_C, point E). Finally, the load P linearly decreases with decreasing δ, due to the increasing embedded length of the fiber (see the generic point F). When the load attains the value—P_P, the fiber is embedded in the matrix for a length l, and the negative translation—δ_P is a result of the elastic compressive deformation of the fiber.

For a non-aligned fiber (that is, when there is an inclination angle α between the fiber and the loading axis, see Fig. 5a), which is the case of randomly distributed fiber composites (see Section 4.2), various studies have indicated an increase of the peak load P_P with increasing α. As was originally proposed by Morton and Groves (1976), we can assume:

$$P_P(\alpha) = \pi D_f l \tau_0 e^{f\alpha} \tag{20}$$

(instead of P_P given in Eq. (15)), where f is the so-called snubbing coefficient whose value usually ranges from 0.7 to 0.9.

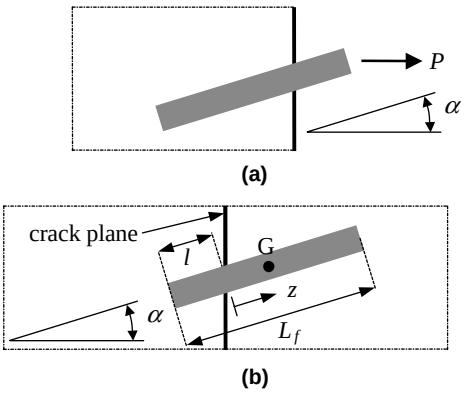

Fig. 5. (a) Position of the generic fiber with respect to the loading axis (direction of the pull-out load P). (b) Position of the generic fiber with respect to the crack plane (G = fiber centroid).

4.2. Randomly distributed short-fiber composites

Let us examine a crack in the matrix of a composite material with randomly distributed short fibers (i.e. fibers with $L_f \leqslant (\sigma_f D_f)/(2\tau_0)$, since we have to pose $2l = L_f$ in Eq. (19) in this case). For each single fiber intersecting the crack, the relationship between the crack bridging force P and the crack opening translation w might be described by Eqs. (13)–(18), where we should consider that the crack opening translation is equal to twice the pull-out displacement ($w = 2\delta$) and the embedded length l of the fiber is equal to $L_f/2 - z$ (z = distance of the fiber centroid from the crack plane, measured along the fiber axis, see Fig. 5b).

In a continuous approximation (which is reasonable provided that the fiber mean spacing is much smaller that the crack length), a relationship between the crack bridging stress σ, understood as a bridging force per unit crack surface, and the crack opening translation w can be considered, and the related peak crack bridging stress σ_P (corresponding to the initial yield force according to the present elastic–plastic crack bridging model; see Section 4.3) can be determined. Assuming a uniform distribution for the fibers, corresponding to the following probability density functions: $\Pr(\alpha) = \frac{1}{2}\sin\alpha$ and $\Pr(z) = 1/L_f$, we have (Li, 1992):

$$\sigma_P = \frac{16}{\pi D_f^2} V_f \int_0^{\pi/2} \int_0^{L_f/2} \pi D_f \left(\frac{L_f}{2} - z\right) \tau_0 \frac{1}{L_f} e^{f\alpha} \frac{\sin\alpha}{2} \, dz \, d\alpha \tag{21}$$

Integration of Eq. (21) yields:

$$\sigma_P = \frac{V_f L_f \tau_0}{D_f} \left(\frac{1 + f e^{f\pi/2}}{1 + f^2}\right) \tag{22}$$

4.3. Link to the proposed crack bridging model

The cyclic pull-out behaviour of a single aligned fiber (see Fig. 4) can be used to characterise the crack bridging behaviour of a fibrous composite. Accordingly, the relationship between the crack bridging stress σ (with a peak value σ_P given by Eq. (22)) and the crack opening translation w can be described by a diagram similar to the P–δ one in Fig. 4.

In order to employ the crack bridging model proposed in Section 2, a discretisation is needed so that the approximately continuous bridging action distribution can be replaced by a discrete distribution of equiv-

alent bridging forces. Assuming a constant relative spacing $\Delta\zeta = (c_{i+1} - c_i)/b$ (with $i = 1, \ldots, n-1$) for the equivalent reinforcements, the initial yield force (related to the peak value σ_P of the crack bridging stress) for each reinforcement is:

$$F_P = \sigma_P b t \Delta\zeta \tag{23}$$

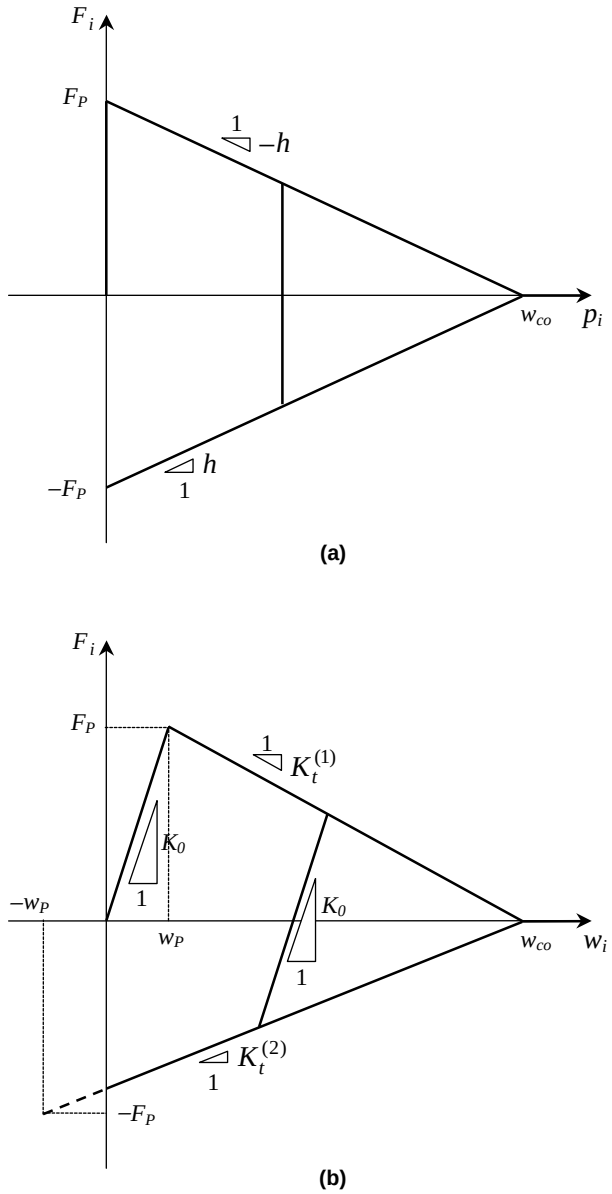

Fig. 6. Elastic–plastic model with linear isotropic tensile softening/compressive hardening describing the short-fiber bridging behaviour of the equivalent ith reinforcement: (a) bridging force F_i against plastic crack opening translation p_i; (b) bridging force F_i against total crack opening translation w_i.

Such a value is constant for all the n equivalent reinforcements activated by the crack (Fig. 1). Note that the spacing $\Delta\zeta$ might be related to the actual fiber spacing (although this is not the case for randomly distributed short-fibers) or to the diameter of the fiber–matrix unit cell (Fig. 4).

The crack bridging law of short fibers is then described by a specialised version of the proposed elastic–plastic model, namely by taking $\kappa_i = 1$ (isotropic hardening) and $-h_i^{(1)} = h_i^{(2)} > 0$ (tensile softening/compressive hardening) in Eq. (1). As is shown in Fig. 6a (reporting the relationship between the bridging force and the plastic crack opening translation), $-h_i^{(1)} = h_i^{(2)} = h = F_P/w_{co}$ with $w_{co} = L_f$ (see Eq. (18) with $\delta_{co} = w_{co}/2$ and $l = L_f/2$). Then, by posing $\delta_P = w_P/2$ and $l = L_f/2$ in Eq. (16), we obtain:

$$w_P = (L_f^2 \tau_0)/[(1+\eta)E_f D_f] \tag{24}$$

Finally, for the values of F_P, w_{co} and w_P being determined as discussed above, the stiffnesses K_0, $K_t^{(1)}, K_t^{(2)}$ can easily be computed (see the diagram in Fig. 6b, reporting the relationship between the bridging force and the total crack opening translation).

5. Illustrative numerical examples

Consider a rectangular cross-section of a fiber-reinforced concrete beam with $t = 0.2$ m, $b = 0.3$ m, submitted to a pulsating cyclic bending ($M_{min} = 0$). The concrete mechanical properties E and K_{IC} are assumed to be equal to 32.1 GPa and 1.75 MPa $\sqrt{m}$, respectively. Further, in the present section, the concrete compressive strength is assumed to be as high as to avoid crushing failure, that is, failure is supposed to be caused by unstable fracture of the matrix.

The fibers, randomly distributed in the cementitious matrix, are characterised by a Young modulus $E_f = 200$ GPa, a frictional bond stress $\tau_0 = 2$ MPa, a snubbing factor $f = 0.7$ and an aspect ratio $L_f/D_f = 50$. Two types of fibers are considered: the first one (e.g. typical of steel fibers) is characterised by a diameter $D_f = 480$ μm ($L_f = 24$ mm), the second one (e.g. typical of carbon fibers) is characterised by a diameter $D_f = 48$ μm ($L_f = 2.4$ mm). Both fiber types are characterised by a tensile strength σ_f (300 and 3000 MPa for steel fibers and carbon fibers, respectively) as high as to avoid fiber failure (short-fiber range): the dimensionless parameter L_f/b is equal to 0.08 for the first type (steel fibers), and to 0.008 for the second type (carbon fibers).

Three values of the fiber volume fraction V_f are considered: 0.6%, 1.2% and 2.4%. The resulting values of the peak crack bridging stress σ_P obtained from Eq. (22) are equal to 1.28, 2.56 and 5.12 MPa, respectively. By adopting the following dimensionless form:

$$\tilde{\sigma}_P = (\sigma_P b^{0.5})/K_{IC} \tag{25}$$

we have $\tilde{\sigma}_P = 0.4$, 0.8 and 1.6 for the above three values of the fiber volume fraction.

Note that the value of the parameter η (Eq. (14)) ranges from 3.8 to 15.6% as the fiber volume fraction V_f varies. In the following, in order to consider for each type of fibers the same value of w_P regardless of the V_f value (see Eqs. (14) and (24)), η is taken as equal to zero (stiff matrix hypothesis; e.g. see Li, 1992). The parameter w_P is equal to 12 and 1.2 μm for the steel fibers and the carbon fibers considered, respectively. The values of $w_{co} = L_f$ are equal to 24 and 2.4 mm for the steel fibers and the carbon fibers considered, respectively.

In the ensuing numerical examples, a discretisation corresponding to 5% of b is adopted ($\Delta\zeta = 0.05$ in Eq. (23)), which corresponds to 20 equivalent reinforcements. The number of cycles in each loading block used to integrate the Paris law is chosen so as to yield a crack depth increment (during fatigue propagation) equal to at least 1% of b ($\Delta\xi = 0.01$).

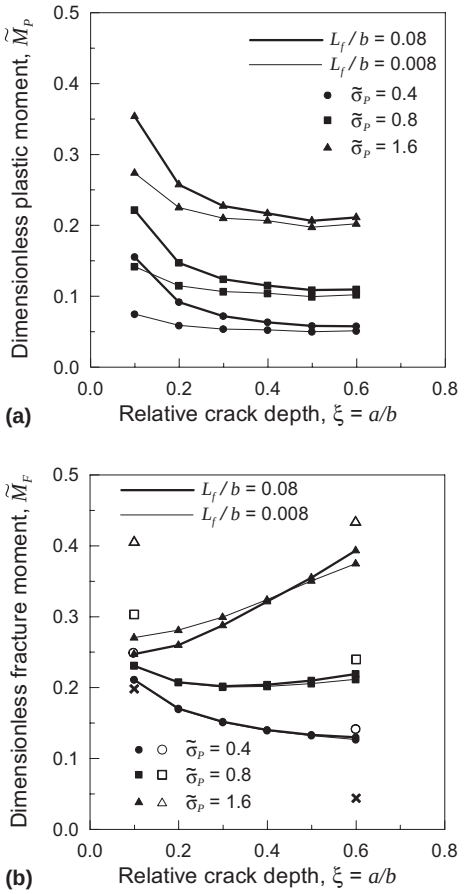

Fig. 7. (a) Dimensionless plastic bending moment $\widetilde{M}_P$ against relative crack depth ξ. (b) Dimensionless unstable fracture bending moment $\widetilde{M}_F$ against relative crack depth ξ (solid symbols). Theoretical values of $\widetilde{M}_F$ at $\xi = 0.1$ and $\xi = 0.6$ for unbridged cracks (×) and bridged cracks with uniform closing stress $\tilde{\sigma}_P$ (hollow symbols) are also reported.

Fig. 7a shows the variation of the dimensionless plastic bending moment $\widetilde{M}_P = M_P/(K_{IC}b^{2.5})$ against the relative crack depth ξ (in the range $0.1 \leqslant \xi \leqslant 0.6$), for different values of L_f/b and $\tilde{\sigma}_P$. It can be seen that $\widetilde{M}_P$ tends to decrease with increasing ξ, and that such a bending moment is smaller for carbon fibers (thin-line curves).

The variation of the dimensionless unstable fracture bending moment $\widetilde{M}_F = M_F/(K_{IC}b^{2.5})$ as a function of the relative crack depth ξ (Fig. 7b) shows different trends of behaviour as $\tilde{\sigma}_P$ varies. In particular, $\widetilde{M}_F$ tends to decrease with increasing ξ for small values of $\tilde{\sigma}_P$, while the opposite occurs for large values of $\tilde{\sigma}_P$. These trends of behaviour are confirmed by the theoretical values of $\widetilde{M}_F$ reported in Fig. 7b for some limiting cases (Tada et al., 1985): an unbridged crack and three bridged crack cases (each bridged crack case is related to a uniform closing stress σ_P corresponding to one of the above three $\tilde{\sigma}_P$ values, respectively).

For the sake of comparison, the predictions of the present model in terms of unstable fracture bending moment are reported in Table 1 together with those of the theoretical model by Matsumoto and Li (1999), for different values of the crack depth. Note that the reported results of Matsumoto and Li refer to the net contribution of fibers to crack bridging, i.e. excluding aggregate bridging contribution. The comparison

Table 1
Dimensionless unstable fracture bending moment $\widetilde{M}_F$ against relative crack depth ξ according to the present model and that by Matsumoto and Li (1999), for different types of fiber-reinforced concrete

Relative crack depth	Present			Matsumoto and Li (1999)		
	SS1	HS1	HS2	SS1	HS1	HS2
0.2	0.14	0.13	0.15	0.12	0.09	0.17
0.4	0.15	0.14	0.20	0.22	0.16	0.32
0.6	0.36	0.28	0.60	0.31	0.21	0.44

SS1 = straight steel fibers with $V_f = 0.01$; HS1 = hooked-end steel fibers with $V_f = 0.01$; HS2 = hooked-end steel fibers with $V_f = 0.02$.

concerns beams with $t = 0.05$ m and $b = 0.1$ m, made of fiber-reinforced concrete with $E = 35$ GPa and $K_{IC} = 0.5$ MPa $\sqrt{\text{m}}$. Three different combinations of type and content of randomly distributed short fibers are considered, that is: straight steel fibers with a volume fraction V_f equal to 1% (termed SS1), and hooked-end fibers with V_f equal to 1% and 2% (termed HS1 and HS2, respectively). Straight fibers are characterised by a diameter $D_f = 400$ μm, a length $L_f = 25$ mm and a frictional bond stress $\tau_0 = 6$ MPa (the snubbing factor f is equal to 0.8), while hooked-end fibers have $D_f = 500$ μm, length $L_f = 30$ mm and $\tau_0 = 4.5$ MPa ($f = 0.75$). The Young modulus E_f of the fibers is equal to 210 GPa. As shown in Table 1, the comparison appears fairly satisfactory, since both the present model and that by Matsumoto and Li (1999) predict the same trend of behaviour.

By juxtaposing Fig. 7a and b, it can be remarked that depending on ξ (and on the parameters L_f/b and $\tilde{\sigma}_P$), the unstable fracture bending moment can be higher or lower than the plastic bending moment.

For carbon fibers ($L_f/b = 0.008$) with $\tilde{\sigma}_P = 0.8$, Fig. 8 illustrates the bridging force distributions along the crack at plastic and unstable fracture bending moments (see Fig. 7) for different values of the relative crack depth ξ.

In Fig. 9, the cyclic bending moment–rotation curves ($\tilde{\varphi}$ = normalised rotation, with $\tilde{\varphi} = \varphi\widetilde{E}$ and $\widetilde{E} = (Eb^{0.5})/K_{IC}$) at different values of ξ are reported for three different cases. For each case, the curves refer to a pulsating bending moment with M_{max} equal to 70% of the corresponding unstable fracture bending moment for $\xi = 0.10$ ($\widetilde{M} = 0.19$ for $\tilde{\sigma}_P = 1.6$ and $L_f/b = 0.008$, Fig. 9a; $\widetilde{M} = 0.15$ for $\tilde{\sigma}_P = 0.4$ and

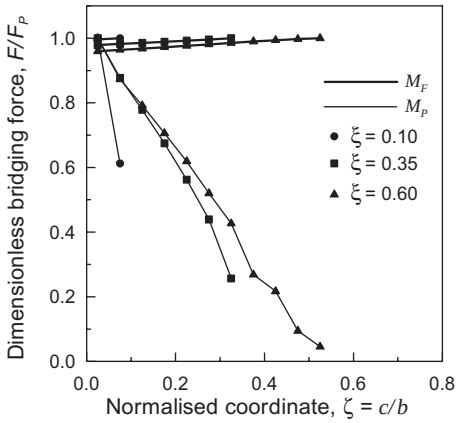

Fig. 8. Dimensionless bridging force F/F_P against relative position ζ along the crack with respect to the bottom of the beam at plastic bending moment M_P and unstable bending fracture moment M_F for different values of the crack depth ξ, carbon fibers ($L_f/b = 0.008$) with $\tilde{\sigma}_P = 0.8$.

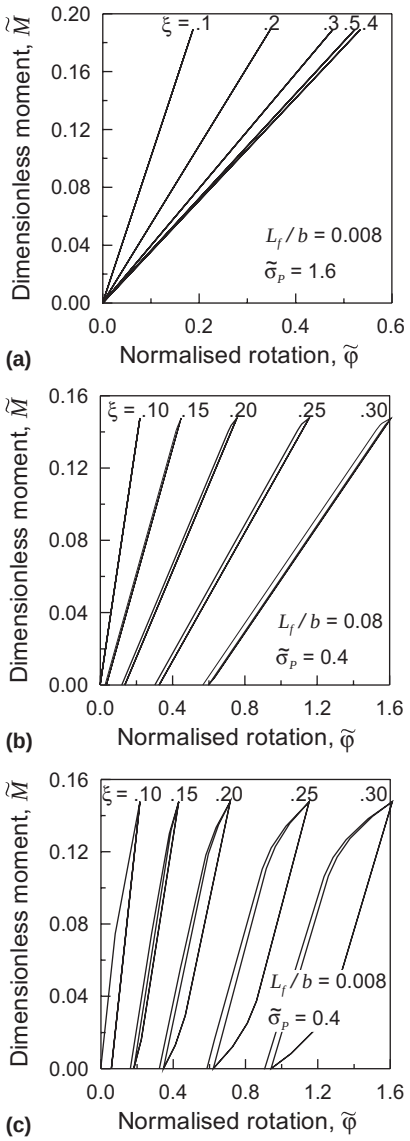

Fig. 9. Cyclic curves of dimensionless bending moment $\widetilde{M}$ against normalised rotation $\tilde{\varphi}$ for $M_{\min} = 0$ and $M_{\max} = 0.7M_{F,0.1}$ ($M_{F,0.1}$ is the unstable fracture moment at $\xi = 0.1$) at different values of relative crack depth ξ: (a) carbon fibers ($L_f/b = 0.008$) with $\tilde{\sigma}_P = 1.6$; (b) steel fibers ($L_f/b = 0.08$) with $\tilde{\sigma}_P = 0.4$; (c) carbon fibers ($L_f/b = 0.008$) with $\tilde{\sigma}_P = 0.4$.

$L_f/b = 0.08$, Fig. 9b; $\widetilde{M} = 0.15$ for $\tilde{\sigma}_P = 0.4$ and $L_f/b = 0.08$, Fig. 9c). The same loading conditions are adopted in Fig. 10. The three regions of behaviour schematically described in Fig. 3 can be encountered as the relative crack depth ξ increases (elastic behaviour in Fig. 9a, elastic shake-down and plastic shake-down in Fig. 9b and c). Note the non-monotonic trend for the flexural stiffness as the relative crack depth increases for the case reported in Fig. 9a. This is due to the effect of the activation of new reinforcements as the crack depth increases.

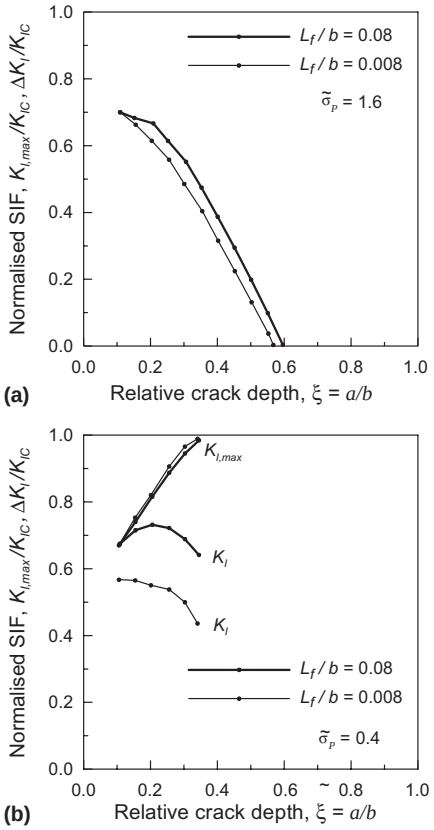

Fig. 10. Maximum value and range of normalised stress intensity factor ($K_{I,max}/K_{IC}$ and $\Delta K_I/K_{IC}$, respectively) against relative crack depth ξ for $M_{min} = 0$ and $M_{max} = 0.7M_{F,0.1}$ ($M_{F,0.1}$ is the unstable fracture moment at $\xi = 0.1$): (a) $\tilde{\sigma}_P = 1.6$ ($K_{I,max} = \Delta K_I$); (b) $\tilde{\sigma}_P = 0.4$.

The cyclic bending moment–rotation curves are reported up to the crack depth corresponding to crack arrest ($\Delta K_I = 0$, Fig. 9a) or to unstable fracture failure ($K_{Imax} = K_{IC}$, Fig. 9b and c). The reason for crack arrest when $\tilde{\sigma}_P = 1.6$, in contrast to that for unstable fracture failure when $\tilde{\sigma}_P = 0.4$, can clearly be observed in Fig. 10, where the maximum value and range of the SIF K_I within a loading cycle at different values of the crack depth ξ are reported. For $\tilde{\sigma}_P = 1.6$ (Fig. 10a), where $K_{Imin} = 0$ (elastic behaviour) and, hence, $\Delta K_I = K_{Imax}$, the range of SIF (governing the crack growth rate according to the adopted Paris law) tends to zero as ξ increases. On the other hand, for $\tilde{\sigma}_P = 0.4$ (Fig. 10b), where $K_{Imin} \neq 0$ (elastic or plastic shake-down) and, hence, $\Delta K_I \neq K_{Imax}$, the range of SIF tends to decrease as ξ increases while its maximum value increases up to K_{IC} (unstable fracture failure).

6. Conclusions

A theoretical model based on fracture mechanics concepts is herein proposed to analyse the fatigue behaviour of a brittle-matrix fibrous composite beam subjected to a constant amplitude cyclic bending. Accordingly, a cracked beam with an elastic matrix and fibers acting as general elastic–plastic bridging ele-

ments is examined. The assumptions of the model allow us to describe typical cyclic phenomena, including elastic shake-down and plastic shake-down, and to predict fatigue life.

It is shown that the cyclic crack bridging behaviour of short fibers (where failure is dominated by sliding phenomena at the fiber–matrix interface) can conveniently be described by an isotropic tensile softening/compressive hardening law, within the general context of the proposed elastic–plastic crack bridging model.

Some composite beams have been analysed in order to show the capabilities of the model. The results are presented in terms of: bending moment against beam cross-section rotation; plastic bending moment, unstable fracture bending moment and stress intensity factor against relative crack depth. It is shown that the fatigue behaviour (leading to unstable fracture failure or crack arrest) is, among others, strongly affected by the dimensionless value of the peak crack bridging stress. A smaller influence of the fiber length is noticed in the cases being considered.

Acknowledgments

The authors gratefully acknowledge the research support for this work provided by the Italian Ministry for University and Technological and Scientific Research (MIUR).

References

Bao, G., McMeeking, R.M., 1995. Thermomechanical fatigue cracking in fiber reinforced metal–matrix composites. J. Mech. Phys. Solids 43, 1433–1460.

Begley, M.R., McMeeking, R.M., 1995. Fatigue crack growth with fiber failure in metal–matrix composites. Compos. Sci. Tech. 53, 365–382.

Carpinteri, Al., 1984. Stability of fracturing process in RC beams. J. Struct. Eng. ASCE 110, 544–558.

Carpinteri, An., 1991. Energy dissipation in RC beams under cyclic loadings. Eng. Fract. Mech. 39, 177–184.

Carpinteri, An., 1992. Reinforced concrete beam behavior under cyclic loadings. In: Carpinteri, Al. (Ed.), Applications of Fracture Mechanics to Reinforced Concrete. Elsevier Science Publishers, UK, pp. 547–578.

Carpinteri, Al., Carpinteri, An., 1984. Hysteretic behavior of RC beams. J. Struct. Eng. ASCE 110, 2073–2084.

Carpinteri, Al., Massabò, R., 1996. Bridged versus cohesive crack in the flexural behaviour of brittle-matrix composites. Int. J. Fract. 81, 125–145.

Carpinteri, Al., Massabò, R., 1997. Continuous vs discontinuous bridged-crack model for fiber-reinforced materials in flexure. Int. J. Solids Struct. 34, 2321–2338.

Carpinteri, Al., Puzzi, S., 2003. Hysteretic flexural behaviour of brittle matrix fibrous composites: the case of two fibers. In: Proceedings of the 16th AIMETA Congress of Theoretical and Applied Mechanics, Ferrara, Italy.

Carpinteri, An., Spagnoli, A., Vantadori, S., 2004. A fracture mechanics model for a composite beam with multiple reinforcements under cyclic bending. Int. J. Solids Struct. 41, 5499–5515.

Carpinteri, An., Spagnoli, A., Vantadori, S., 2005. Mechanical damage of ordinary or prestressed reinforced concrete beams under cyclic bending. Eng. Fract. Mech. 72, 1313–1328.

Chaboche, J.L., 1986. Time-dependent constitutive theories for cyclic plasticity. Int. J. Plasticity 2, 149–188.

Jirasek, M., Bazant, Z.P., 2002. Inelastic Analysis of Structures. John Wiley & Sons Ltd., Chichester, England.

Li, V.C., 1992. Postcrack scaling relations for fiber reinforced cementitious composites. J. Mater. Civil Eng. ASCE 4, 41–57.

Marshall, D.B., Cox, B.N., Evans, A.G., 1985. The mechanics of matrix cracking in brittle-matrix fiber composites. Acta Metall. 33, 2013–2021.

Masing, G., 1926. Eigenspannungen und verfestigung beim Messing. In: Proceedings of the 2nd International Conference of Applied Mechanics, Zurich, pp. 332–335 (in German).

Matsumoto, T., Li, V.C., 1999. Fatigue life of fiber reinforced concrete with a fracture mechanics based model. Cement Concrete Compos. 21, 249–261.

McCartney, L.N., 1987. Mechanics of matrix cracking in brittle-matrix fibre-reinforced composites. Proc. R. Soc. London A 409, 329–350.

McMeeking, R.M., Evans, A.G., 1990. Matrix fatigue cracking in fiber composites. Mech. Mater. 9, 217–227.

Morton, J., Groves, G.W., 1976. The effect of metal wires on the fracture of a brittle matrix composite. J. Mater. Sci. 11, 617–622.

Paris, P.C., Erdogan, F., 1963. A critical analysis of crack propagation laws. J. Basic Eng. 85, 528–534.
Tada, H., Paris, PC., Irwin, G., 1985. The Stress Analysis of Cracks. Paris Productions Incorporated (and Del Research Corporation), St. Louis, MO.
Zhang, J., Stang, H., 1998. Fatigue performance in flexure of fiber reinforced concrete. ACI Mater. J. 95, 58–68.
Zhang, J., Stang, H., Li, V.C., 1999. Fatigue life prediction of fiber reinforced concrete under flexural load. Int. J. Fatigue 21, 1033–1049.